REPORT DOCUMENTATION PAGE

Form Approved OMB NO. 0704-0188

1. REPORT DATE (DD-MM-YYYY)	2. REPORT TYPE	3. DATES COVERED (From - To)
08-02-2015	Final Report	1-Nov-2011 - 31-Oct-2014

4. TITLE AND SUBTITLE

Innovation in Broad-Area Diode Laser Array Architecture: Coupling Grating-Confined Zigzag Modes for High Power, High Brightness Applications

5a. CONTRACT NUMBER
W911NF-11-1-0519

5b. GRANT NUMBER

5c. PROGRAM ELEMENT NUMBER
611102

6. AUTHORS
Lin Zhu

5d. PROJECT NUMBER

5e. TASK NUMBER

5f. WORK UNIT NUMBER

7. PERFORMING ORGANIZATION NAMES AND ADDRESSES
Clemson University
300 Brackett Hall

Clemson, SC 29634 -5702

8. PERFORMING ORGANIZATION REPORT NUMBER

9. SPONSORING/MONITORING AGENCY NAME(S) AND ADDRESS (ES)

U.S. Army Research Office
P.O. Box 12211
Research Triangle Park, NC 27709-2211

10. SPONSOR/MONITOR'S ACRONYM(S)
ARO

11. SPONSOR/MONITOR'S REPORT NUMBER(S)
60283-EL-YIP.6

12. DISTRIBUTION AVAILIBILITY STATEMENT

Approved for Public Release; Distribution Unlimited

13. SUPPLEMENTARY NOTES

The views, opinions and/or findings contained in this report are those of the author(s) and should not contrued as an official Department of the Army position, policy or decision, unless so designated by other documentation.

14. ABSTRACT

This project aims to demonstrate coherent beam combining in a new, completely integrated approach to edge-emitting, high power semiconductor laser emitters and arrays. We have successfully demonstrated integrated mode control and coherent beam combining of high power, broad area lasers through transverse Bragg diffraction. The proposed concept has many advantages over traditional beam combining methods based on discrete and bulky optical components. We have shown that the proposed approach can effectively realize the single mode operation of broad area diode lasers and coherently combine these angled grating lasers with high efficiency

15. SUBJECT TERMS

high power diode lasers, mode control, integrated coherent beam combining

16. SECURITY CLASSIFICATION OF:			17. LIMITATION OF ABSTRACT	15. NUMBER OF PAGES	19a. NAME OF RESPONSIBLE PERSON
a. REPORT	b. ABSTRACT	c. THIS PAGE			Lin Zhu
UU	UU	UU	UU		19b. TELEPHONE NUMBER 864-656-4381

Report Title

Innovation in Broad-Area Diode Laser Array Architecture: Coupling Grating-Confined Zigzag Modes for High Power, High Brightness Applications

ABSTRACT

This project aims to demonstrate coherent beam combining in a new, completely integrated approach to edge-emitting, high power semiconductor laser emitters and arrays. We have successfully demonstrated integrated mode control and coherent beam combining of high power, broad area lasers through transverse Bragg diffraction. The proposed concept has many advantages over traditional beam combining methods based on discrete and bulky optical components. We have shown that the proposed approach can effectively realize the single mode operation of broad-area diode lasers and coherently combine these angled-grating lasers with high efficiency.

Enter List of papers submitted or published that acknowledge ARO support from the start of the project to the date of this printing. List the papers, including journal references, in the following categories:

(a) Papers published in peer-reviewed journals (N/A for none)

Received		Paper
02/08/2015	5.00	Yunsong Zhao, Lin Zhu. Folded cavity angled-grating broad-area lasers, Optics Express, (10 2013): 24087. doi: 10.1364/OE.21.024087
08/13/2012	1.00	Yunsong Zhao, Jiahua Fan, Lin Zhu. Modal and scalability analysis of a zigzag array structure for passive coherent beam combining, Journal of the Optical Society of America B, (03 2012): 0. doi: 10.1364/JOSAB.29.000650
08/13/2012	2.00	Lin Zhu, Yunsong Zhao. On-chip coherent combining of angled-grating diode lasers toward bar-scale single-mode lasers, Optics Express, (03 2012): 0. doi: 10.1364/OE.20.006375
08/26/2013	3.00	Lin Zhu, Yunsong Zhao. Improved Beam Quality of Coherently Combined Angled-Grating Broad-Area Lasers, IEEE Photonics Journal, (04 2013): 0. doi: 10.1109/JPHOT.2013.2245884
TOTAL:	**4**	

Number of Papers published in peer-reviewed journals:

(b) Papers published in non-peer-reviewed journals (N/A for none)

Received		Paper
TOTAL:		

Number of Papers published in non peer-reviewed journals:

(c) Presentations

Number of Presentations: 0.00

Non Peer-Reviewed Conference Proceeding publications (other than abstracts):

Received	Paper

TOTAL:

Number of Non Peer-Reviewed Conference Proceeding publications (other than abstracts):

Peer-Reviewed Conference Proceeding publications (other than abstracts):

Received	Paper	
09/01/2014	4.00	Mark S. Zediker, Yunsong Zhao, Lin Zhu. Integrated coherent beam combining of a laser diode mini-bar, SPIE LASE. 07-FEB-14, San Francisco, California, United States. : ,

TOTAL: **1**

Number of Peer-Reviewed Conference Proceeding publications (other than abstracts):

(d) Manuscripts

Received	Paper

TOTAL:

Number of Manuscripts:

Books

Received Book

TOTAL:

Received Book Chapter

TOTAL:

Patents Submitted

Patents Awarded

Awards

Yunsong Zhao Hitachi High Technologies America Electron Microscopy Fellowship

Graduate Students

NAME	PERCENT SUPPORTED	Discipline
Yunsong Zhao	0.80	
Jiahua Fan	0.30	
Ruoyu Zhang	0.20	
FTE Equivalent:	**1.30**	
Total Number:	**3**	

Names of Post Doctorates

NAME	PERCENT_SUPPORTED
FTE Equivalent:	
Total Number:	

Names of Faculty Supported

NAME	PERCENT_SUPPORTED	National Academy Member
lin zhu	0.33	
FTE Equivalent:	**0.33**	
Total Number:	**1**	

Names of Under Graduate students supported

NAME	PERCENT_SUPPORTED
FTE Equivalent:	
Total Number:	

Student Metrics

This section only applies to graduating undergraduates supported by this agreement in this reporting period

The number of undergraduates funded by this agreement who graduated during this period:	2.00
The number of undergraduates funded by this agreement who graduated during this period with a degree in science, mathematics, engineering, or technology fields:.....	2.00
The number of undergraduates funded by your agreement who graduated during this period and will continue to pursue a graduate or Ph.D. degree in science, mathematics, engineering, or technology fields:.....	2.00
Number of graduating undergraduates who achieved a 3.5 GPA to 4.0 (4.0 max scale):.....	2.00
Number of graduating undergraduates funded by a DoD funded Center of Excellence grant for Education, Research and Engineering:.....	0.00
The number of undergraduates funded by your agreement who graduated during this period and intend to work for the Department of Defense	2.00
The number of undergraduates funded by your agreement who graduated during this period and will receive scholarships or fellowships for further studies in science, mathematics, engineering or technology fields:	0.00

Names of Personnel receiving masters degrees

NAME	
Ruoyu Zhang	
Total Number:	**1**

Names of personnel receiving PHDs

NAME
Total Number:

Names of other research staff

NAME	PERCENT SUPPORTED
FTE Equivalent:	
Total Number:	

Sub Contractors (DD882)

Inventions (DD882)

Scientific Progress

see attachments

Technology Transfer

Final report: Innovation in Broad-Area Diode Laser Array Architecture: Coupling Grating-Confined Zigzag Modes for High Power, High Brightness Applications

Project number: W911NF-11-1-0519

Summary

This project aims to demonstrate coherent beam combining in a new, completely integrated approach to edge-emitting, high power semiconductor laser emitters and arrays. Through this project, we have experimentally demonstrate a number of novel integrated modal control and beam combining methods for high power, high brightness semiconductor laser diodes, including: 1) Waveguide mode selection has been achieved through angled transverse Bragg grating approach that creates >100 micron wide lasers with a single transverse mode, and two such lasers have been combined (through two dimensional Bragg diffraction) in a "V" pattern to create a diffraction-limited beam. The coherence has been verified via double slit interference pattern created at the "V" side where the two separate lasers emit; 2) We improve the beam quality and performance of coherently combined angled-grating broad-area lasers through ion implantation. We show that the nonuniform current/gain distribution in our first-generation lasers excites the second order Bragg mode and degrades the beam quality. Ion implantation is used to provide a more uniform current distribution by confining the injected current within the grating area. The far-field measurement result shows that the near-diffraction-limited, single lobe envelope is obtained. Smaller threshold and larger slope efficiency are observed in the L-I curve as well; 3) We demonstrate integrated coherent beam combining of a mini laser bar with six angled-grating broad-area lasers and obtain near diffraction-limited beam quality of the combined bar. The adjacent angled-grating broad-area lasers in the mini-bar array have opposite tilt directions and overlap at one facet. Coherent beam combining is obtained through Bragg diffraction in 2D photonic crystal coupling regions defined by overlapped areas. The combined mini-bar shows high contrast ratio interference patterns in the far field, indicating excellent spatial coherence among all six emitters. In addition, the optical spectra of each individual emitting aperture show the same lasing wavelengths. The light-current (L-I) curve of the combined mini-bar is also presented. The highest output power is limited by the thermal effect. Our results constitute an important step towards achieving fully-integrated, bar-scale single mode high power diode lasers.

1. Project Motivation

Standard high power diode laser bars consist of a one dimensional array of single broad-area emitters placed side by side [1, 2]. While this conventional design can provide up to 1KW output power [3], the beam quality in the horizontal direction is very poor, usually about a thousand times worse than the diffraction limit. This has become the limiting factor for diode laser bars to become efficient direct-energy/pumping sources with high beam quality. Our YIP proposal describes an innovative zigzag supercavity architecture that can provide diffraction-limited beam quality for high power, broad-area diode bars. Importantly, our approach does not require any external optical components or differential phase feedback mechanism and thus will greatly reduce the system complexity and cost. The successful realization of this transformative research would have enormous long-term impacts on laser weapons, laser radar systems, and the national needs.

Semiconductor diode lasers provide many unique advantages over other laser systems, such as a wide range of operation wavelengths, high electrical to optical conversion efficiency, high compactness, and low cost [4-8]. On the negative side, high power, high brightness (diffraction-limited beam quality) operation is difficult to obtain due to highly nonlinear materials and strong coupling between gain and

index [9, 10]. Today, broad-area diode lasers are usually used for high power applications, such as material processing and pumping sources for solid-state and fiber lasers. A few watts output power can be obtained from a single emitter (100μm wide and 1mm long) and a few hundred watts output power can be obtained from a laser bar that consists of a 1D array of broad-area lasers. Due to lack of transverse mode control and strong nonlinear effects, these high power sources exhibit very poor beam quality and cannot provide the desired high brightness.

In order to obtain high power, diffraction-limited output beam from a diode laser bar, we need to solve a two-fold problem: First, each broad-area single emitter should operate in a single-transverse mode; Second, all the emitters on the bar should be combined without reducing their beam quality. For a step-index waveguide laser, its width has to be less than a few microns in order to obtain the single transverse mode operation to maintain good beam quality. This limits the laser output power less than a few hundred miliwatts. There are a variety of techniques to obtain a large aperture single transverse mode diode laser. Depending on if external optical components are needed, these techniques can be divided into two categories. The first category can be monolithically implemented, including: 1) evanescently coupled laser arrays, where multiple narrow single transverse mode lasers are coupled together to form a super transverse mode [11-15]; 2) chirped and Y-coupled laser arrays [16-18]; 3) leaky wave coupled (anti-guided) laser arrays [7, 19-21]; 4) unstable resonators, e.g., curved mirror or tapered lasers [22-26]. These unstable resonators can be designed as either independent lasers or amplifiers in master oscillator power amplifier (MOPA) configuration [27-29]; 5) grating confined broad area lasers (α-DFB) [30-40], where angled gratings are used to select a single transverse mode and provide strong modal discrimination. The second category requires external optical components and includes externally injection locked laser arrays [41, 42], external cavity laser arrays through diffractive coupling [43-45], and discrete MOPA lasers [46-48]. By use of these mode control techniques, we can obtain a few watts diffraction-limited output power. Further increasing of the optical power in a single emitter is limited by Catastrophic Optical Damage (COD) and stability/thermal problems.

As for beam combining, it is very challenging to come up with a monolithic solution since the frequency and/or phase of each laser need to be precisely controlled. There are two main beam combining techniques: coherent beam combining (CBC) and spectral beam combining (SBC) [49-51]. SBC systems rely on an external diffractive component to spatially overlap beams from different lasers which operate at different wavelengths [52-54]. In CBC systems, all the lasers operate at the same wavelength and are phase-locked [55-57]. Currently, most beam combining systems are based on the MOPA configuration with active feedback. A single frequency laser output is split and amplified, e.g., by high power fiber amplifiers. The phase of each individual amplified beam is controlled by a discrete optical phase modulator. The phase difference among the array elements is detected and then fed-back to control the phase modulator in order to phase lock all the beams. Although these systems can provide high diffraction-limited power, they are complex, bulky, and expensive.

The objective of the YIP proposal is to demonstrate an innovative integrated laser array architecture that could provide broad-area, single-mode emitters and coherently combine them at the same time. We aim to obtain diffraction-limited, coherently combined optical power directly from a single laser bar without any external optical components or differential phase feedback mechanisms. Specifically, we use the angled grating confined broad area laser [31-40] as the building element. The grating works as an integrated spatial filter and provides single transverse mode operation. By evenly arranging two symmetric grating confined laser arrays with opposite tilt angles, we can obtain the direct optical coupling, induced by facet reflection and Bragg diffraction, between any two adjacent elements. It is the direct optical coupling that coherently combines all the laser elements. The whole structure can be also considered as a folded supercavity in which all the lasers achieve mutual coherence. In this sense, our

approach turns a laser bar that usually consists of many incoherent broad area lasers with poor beam quality into a coherent supercavity laser with diffraction-limited beam quality.

2. Integrated beam combining of two angled-grating broad area lasers

Figure 1 shows a schematic of the coherently combined angled-grating laser. Our laser device is fabricated in an InP-based multiple quantum well (MQW) epitaxy wafer. The combined laser cavity consists of two sets of angled-gratings that tilt to opposite directions with the same angle. The overlap area of the two gratings defines a two dimensional coupling region. The phase locking of two emitters is obtained by the wave coupling through Bragg diffraction in this overlap region. The resonance wavelength is chosen to be around 1550nm. To effectively couple two emitters and reduce modal loss in gratings, the tilt angle θ is set to be 10°. Accordingly, the period of gratings can be calculated to be 1.368μm. The dimensions of a single emitter are 1.3mm×130μm (L×W). The etch depth of 1.0μm is chosen to obtain a grating coupling coefficient around 0.1/μm. Light is confined by gratings transversely and by total internal reflection vertically.

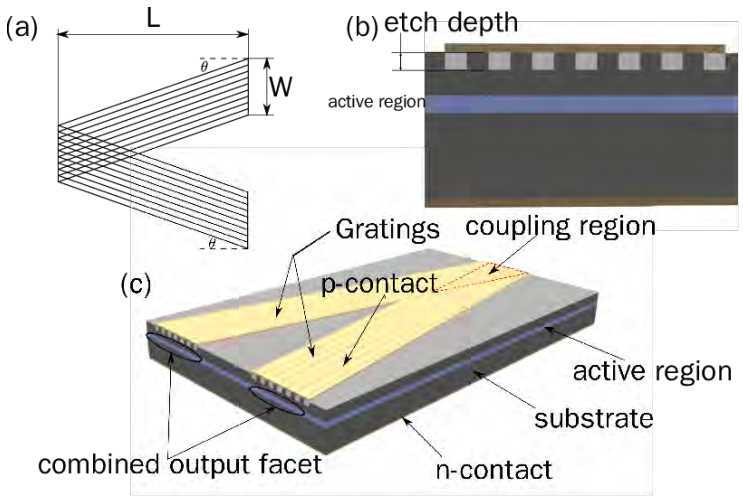

Figure 1 Schematic of a coherently combined angled-grating laser. (a) L and W are the length and width of a single emitter, respectively. θ is the tilt angle of the grating. (b) The cross section structure. (c) Planar geometry of the combined angled-grating laser. Two coherently combined emitters (two legs in the coupled structure) constructively interfere in the far field.

The fabrication process consists of a series of steps of lithography, etching, planarization and metallization. First, a SiO2 layer is deposited by PECVD as a hard mask. Then the grating structure is defined by ebeam lithography. After two steps of dry etching, the gratings are finally transferred to the epiwafer. Next, the structure is planarized by spinning a layer of BCB and then it is etched back until the epiwafer surface exposes. After a SiO2 insulation layer is deposited and a contact window is opened, the p-side metal contact is deposited by an Ebeam evaporator. Then the whole chip is thinned and n-side metal contact is deposited. After the chip is cleaved to a desired length, the laser diode is mounted and wired on a c-mount for measurement. Figure 2 shows the scanning electron microscope (SEM) pictures of the gratings and the packaged laser diode.

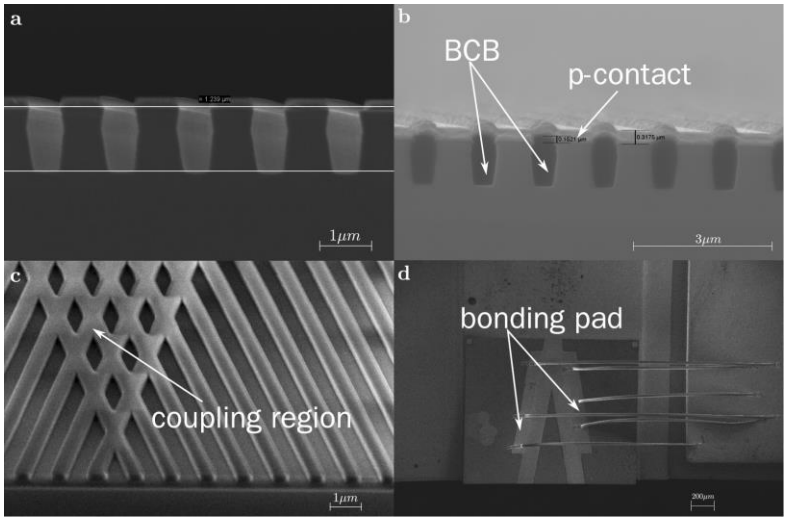

Figure 2 Scanning Electron Microscope images of the combined angled-grating laser.

The measurement results of the L-I curve, spectrum, near field and far field shown in this section are obtained in a cryostat system with the heat sink temperature set at 230K. In all the measurements, the lasers are electrically pumped in CW operation.

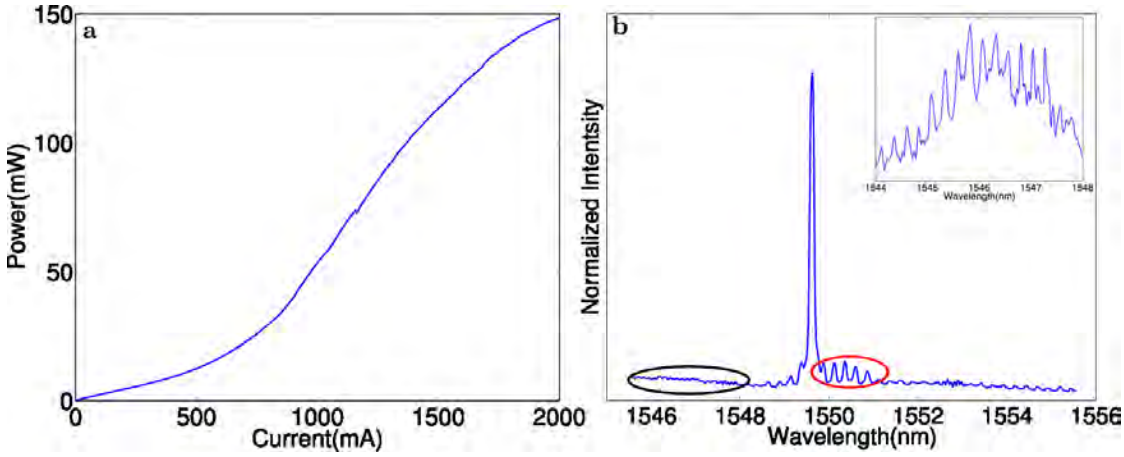

Figure 3 Measurements of the light-current curve and optical spectrum. (a) L-I curve of the combined angled-grating laser. (b) Spectrum of the laser diode when the injection current is 1200mA. The inset is a zoomed-in spectrum in the black circle.

L-I curve and optical spectrum: Figure 3(a) shows the light-current curve of the combined angled grating laser. The threshold current is around 700mA and the slope efficiency is about 0.12W/A. The relatively low slope efficiency indicates high optical loss in the cavity which is mainly caused by the roughness of the gratings induced during the dry etching process. Figure 3(b) shows the optical spectrum of the same laser diode. The pump current is 1200*mA* which is about 1.7*Ith*. The peak wavelength is 1549.62*nm* close to the designed grating resonance wavelength. The inset shows a zoomed-in spectrum from 1544*nm* to 1548*nm* indicating a free spectrum range (FSR) of 0.22*nm*, in agreement with the cavity length of 1.3*mm*. The FSR suggests that the longitudinal modes are defined by two end facets. Longitudinal mode competition is observed around the peaks in the red circle at different current injection levels. The proposed laser diodes usually operate with multiple longitudinal modes, because the gratings here only control the transverse mode and leave the longitudinal dimension free.

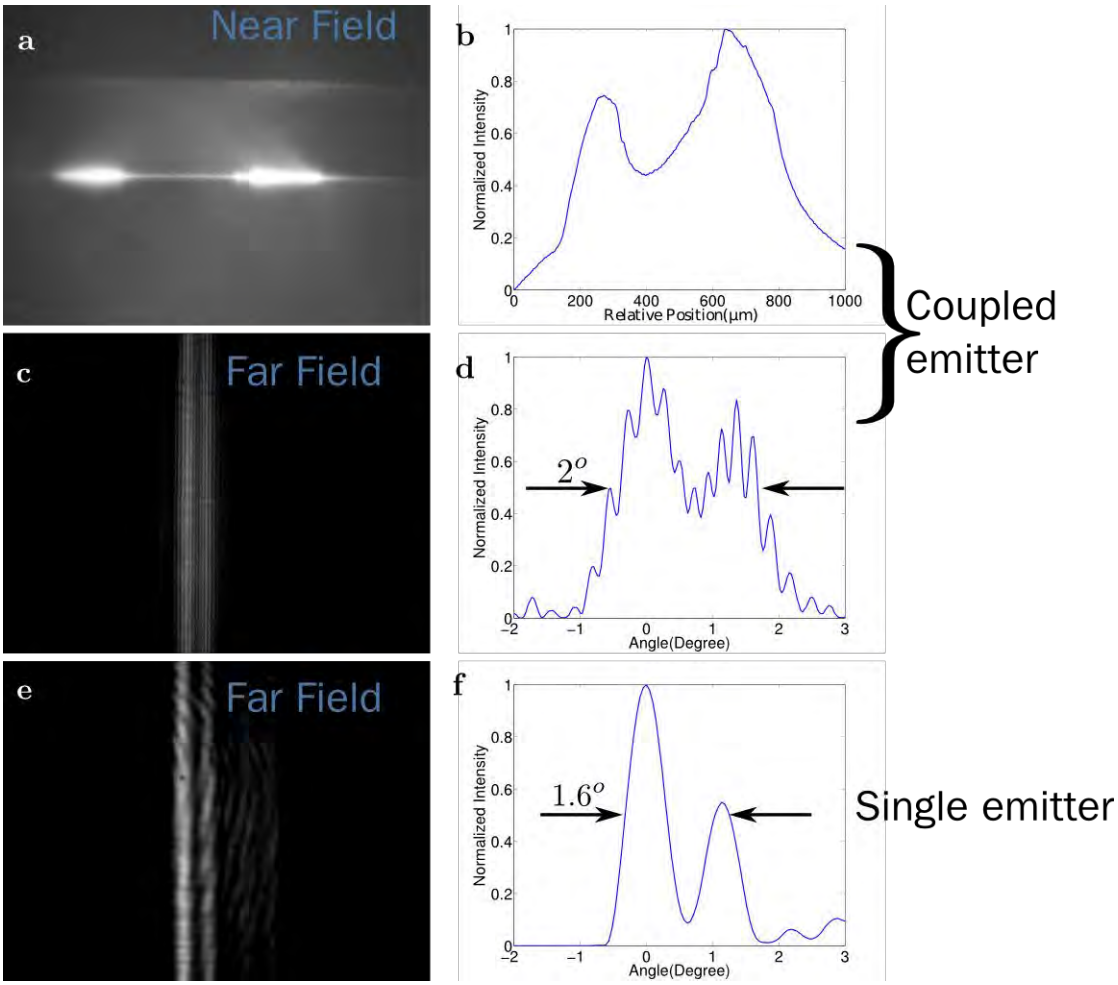

Figure 4 Measurements of the near field and far field of the coupled emitter and single emitter. (a, b) The near field image and profile of the coupled emitter; (c, d) The far field image and profile of the coupled emitter; (e, f) The far field image and profile of a single emitter.

Near field and far field: Figure 4(a) and (b) show the near-field image and profile of the combined angled-grating laser. It is clear that there are two emitting regions along the facet. The difference between the intensities of the two regions comes from the nonuniformity in the wafer and induced by the fabrication processes. The distance between the two emitting regions (368μ*m*) and the emitting width of each region (106μ*m*) indicates that light indeed emits from the designed angled-grating areas. The area between two emitters is illuminated a little bit due to the current leakage. The far field of the same coupled laser is shown in Fig. 4(c) and (d). We compare the far field profile of the combined laser with an uncoupled single emitter. If two coupled emitters are coherently combined and in-phase, they will constructively interfere in the far field and the overall envelop of the interfered far field remains the same as that of a single emitter. The only difference is that within the overall envelop, interference patterns present. This is exactly our measurement results, as shown in Fig. 4 (c-f). The uncoupled single emitter was fabricated on the same chip with the combined laser. The grating parameters such as the period, duty cycle, and total width are also the same. It is clear that the overall envelop of the combined laser's far field is very similar to that of the uncoupled single emitter. The fine interference patterns in Fig. 4(c) and (d) prove that two emitters are coherently combined. The two lobes in the far field come from the degeneracy of two band-edge modes of the grating since the grating etched depth is bigger than the designed value. Single-lobe far field can be obtained by introducing a central defect or 2D

photonic crystal structure or by decreasing the coupling strength of the gratings. The FWHM divergence angles (1.6° for the single emitter and 2° for the combined laser) of these two lasers are still much smaller than a conventional broad-area laser (~10°). The difference in the divergence angles between the single emitter and coupled emitters are mainly due to different near-field distribution induced by the non-uniformity of fabrication and current injection.

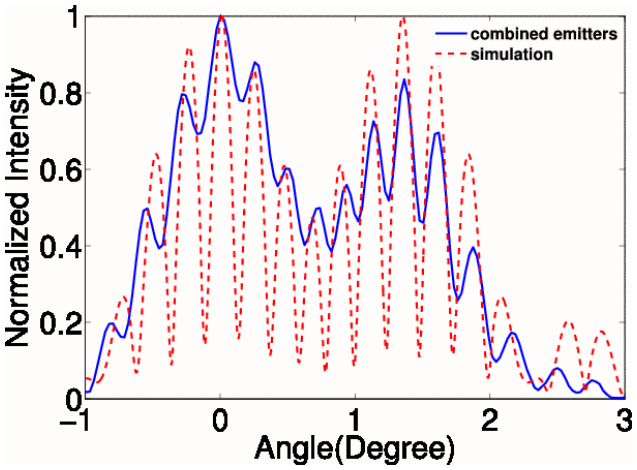

Figure 5 Far-field profiles of the coherently combined laser and simulation result. Solid line presents the measurement result of the coherently combined laser and the dash line is the simulation result.

We extracted the distance between two emitters and the width of one emitter from the measured near field in Fig. 4(a). We assumed that the two emitters were in phase and calculated the far-field pattern by use of the standard diffraction theory. The calculation result is shown in Fig. 5 in the red dashed line and agrees well with the measured result. The angular distance between two interference stripes in the measurement result is 0.246° and it is 0.234° in the calculation. Steady interference patterns are observed when we increase the pump current up to 2*A*, which proves that the combining approach is still effective under a high pump condition.

In summary, we have demonstrated a new type of on-chip coherently combined angled-grating broad-area lasers. Simultaneous modal control and coherent combining are achieved through Bragg diffraction in the proposed laser. Our measurement results of the near field and far field show that two angled grating broad-area lasers are coherently combined and provide near-diffraction-limited output without any external optical components. Our design can be expanded to a coherently combined broad-area laser array, which makes our laser architecture a promising candidate to obtain high power, high brightness bar-scale single mode diode lasers.

3. Improve the beam quality of the coherently combined broad-area lasers

In our previous demonstration, two angled-grating broad-area lasers are phase-locked through Bragg diffraction in an integrated two dimensional (2D) photonic crystal coupling region. More importantly, our design could be expanded to a bar-scale coherently combined laser array. However, the far-field profile reported (shown in Fig.5) has an overall double lobe envelope and the contrast ratio of the interference fringes is low.

In this section, we show that the double lobe envelope of the far-field comes from the second order Bragg mode. It is excited by the nonuniform current/gain distribution due to the lateral current leakage. Here we use ion implantation to confine the current in the grating area so that the fundamental Bragg mode will be the preferred lasing mode. We measure the near fields and far fields of the combined laser diodes. The far-field profile has a single lobe envelope with near diffraction limited divergence angle. We compare the measured interference pattern with the theoretically calculated result and they show good agreement with each other. Compared to our previous result, a better contrast ratio of the interference fringes is obtained. We also measure the output light power versus pump current (L-I) curves and spectra. Smaller threshold and larger slope-efficiency are observed in the ion implanted diodes due to better current confinement.

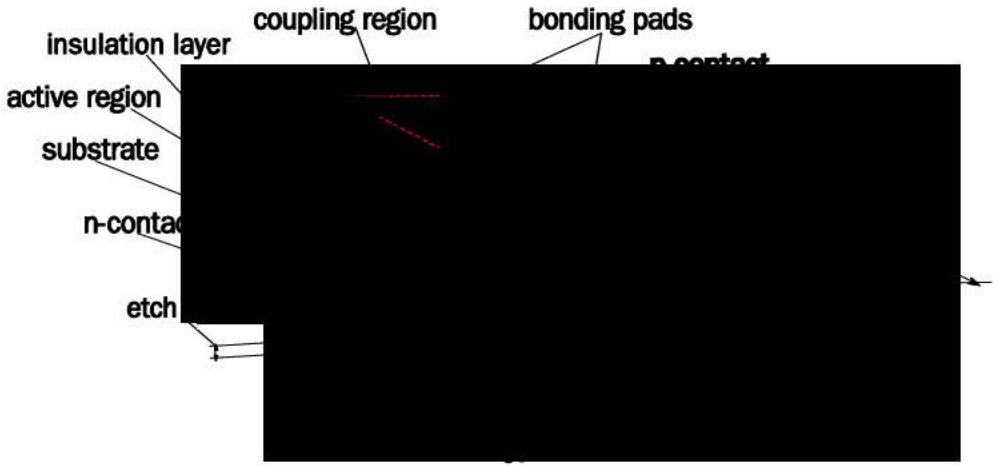

Figure 6 Schematic plot of the coherently combined angled grating lasers. L is the length of cavity, W is the width and θ is the tilting angle. The etched gratings are planarized by BCB. The blue area on top represents the ion-implanted region.

Figure 6 shows the schematic plot of our coherently combined angled-grating broad-area laser integrated on a single chip. The laser cavity consists of two angled-grating broad-area lasers that tilt to opposite directions and overlap at one facet. The overlapped area defines a 2D photonic crystal coupling region that coherently combines the two elements through Bragg diffraction. θ is the tilting angle, *L* and *W* are the cavity length and output aperture width, respectively. The blue area on top represents the ion-implanted region. The wafer structure and fabrication procedure are described in the last section. There are slight changes in our current wafer structure. The thickness of the InP cladding layer is reduced to 1000*nm* and that of the p-contact layer is changed to 20*nm*. Thus, we can obtain the same coupling coefficient with smaller grating etch depth. For fabrication, the gratings are first written on the wafer surface by the ebeam lithography and then transferred into the wafer by dry etching. Before evaporating the metal contacts, the etched gratings are planarized by BCB to prevent metal falling into gratings and then the BCB is etched back to expose the unetched p-contact layer. After the p-side metal contact is evaporated, we implant protons in the blue regions shown in Fig. 1. The tilting angle is set to be 10 degree. We use the first order gratings with the period of 1.3663μ*m* corresponding to the wavelength of 1550*nm* (the effective index is estimated to be 3.2665). The grating etch depth is about 700*nm*. The length of the cavity is about 1.3*mm* after cleaving and the width of a single emitter is about 140μ*m* corresponding to 100 grating periods. The fabricated diodes are die bonded on C-mounts in the p-side up configuration for measurement.

The planarization material, BCB, is electrically isolated. Therefore, the effective resistance of the grating area under the metal contact is larger than that of the p-type highly doped area outside the gratings. As a result, the injected current will concentrate at the edges of the grating area. We carried out a 3D current distribution simulation for a single emitter. In the simulation model, all the interfaces contacting with BCB are set to be electrically isolated and all the other materials are set to have the same conductivity for simplicity. A gold plate is placed right on the top of the gratings as the metal contact. And a current source is set on it. Figure 7(a) shows the top view of the current distribution at the position of the quantum well region. The result shows a nonuniform current distribution with less current at the center and more current at the edges. We show the mode profile of the second and first order (fundamental) Bragg mode in Fig. 7(c) and (d), respectively. They are calculated by a transfer matrix method. It is clear that the second order Bragg mode has a better overlap with this uneven current distribution. Therefore, it is preferred to be the lasing mode instead of the first order mode,

leading to the overall double lobe envelope in the far field. To excite the fundamental Bragg mode, a uniform current distribution is needed. A simple way to accomplish this is to increase the resistance of the area outside the gratings so that the current will be confined within the grating area. Figure 2(b) shows a more uniform current distribution after introducing a higher resistance material to the area outside the gratings. Experimentally, we use ion implantation to increase the resistance outside of the grating region. We first tested several ion implantation recipes with different ion energies in broad-area lasers. Figure 8 shows the near-field results of different recipes. As the ion energy increases, the tails of the emitting aperture become smaller which indicates weaker current leakage. As a result, we choose 260*KeV* proton with the dose of $5 * 10^{14}/cm^2$ as our ion implantation recipe.

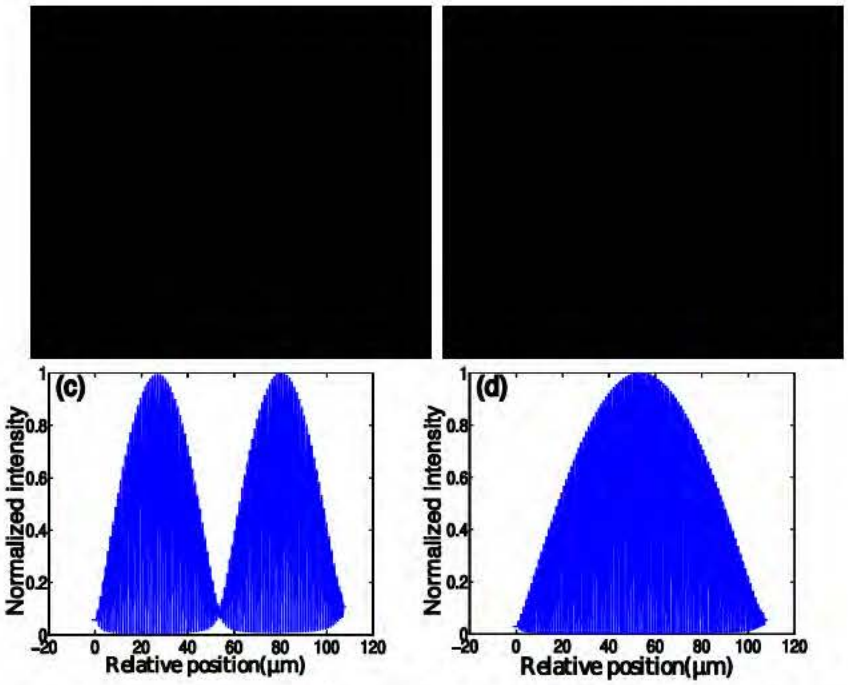

Figure 7 Simulation results of the injected current distribution. (a) Nonuniform current distribution without ion implantation. (b) The distribution becomes more uniform after increasing the resistance outside the grating area. (c) and (d) Electric fields of the second order and first order Bragg modes, respectively.

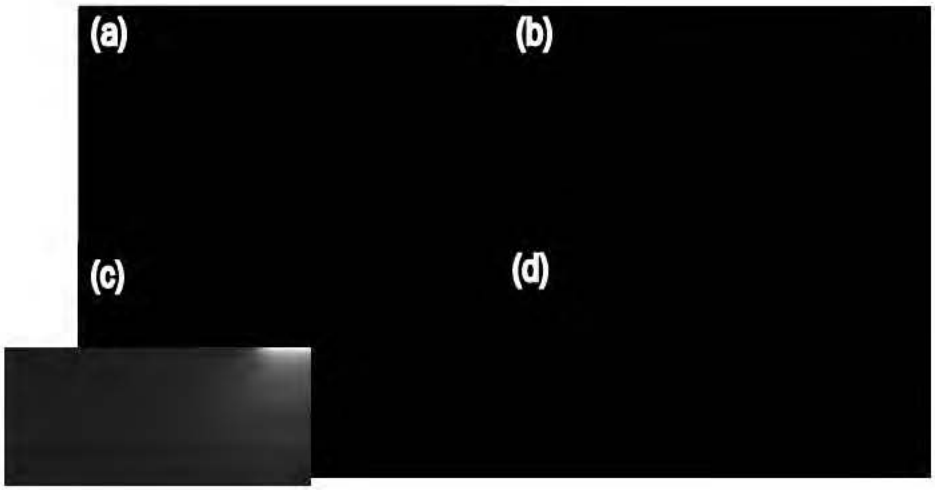

Figure 8 Near field images after proton implantation at different energies with the dose of 5 × 1014/cm2. (a) Not implanted. (b) Ion energy is 180KeV. (c) Ion energy is 220KeV. (d) Ion energy is 260KeV

We measure the completed laser under CW pump condition in a cryostat with the heat sink temperature set at 230K. Figure 9 shows the near field and far field measurement results of our laser. In the near field shown in Fig. 9(a), the total width of the emitting aperture is about 160μm and the distance between the two apertures is about 425.6μm. There is about 10% difference in the intensities of the two beams. These values will be used in the theoretical far-field calculation. Compared with the near field reported in the last section, the near-field profile of the ion implanted lasers has sharper edges of the emitting apertures and larger distinction ratio between the emitting area and dummy area due to better current confinement. In the far field shown in Fig. 9(b), an overall single lobe envelope is obtained. Multiple fringes in the far field are due to the interference of two coherently combined emitters. The full width at half maximum (FWHM) is about 1.08°. The angular distance between fringes is about 0.2073°. Compared with our previous far-field result, a much better contrast ratio of the interference fringes is obtained. The difference between peaks and valleys for our previous device is only about 0.2 and in our current device, the difference is improved to be 0.9 in the normalized scale, which indicates better coherence of the two emitters.

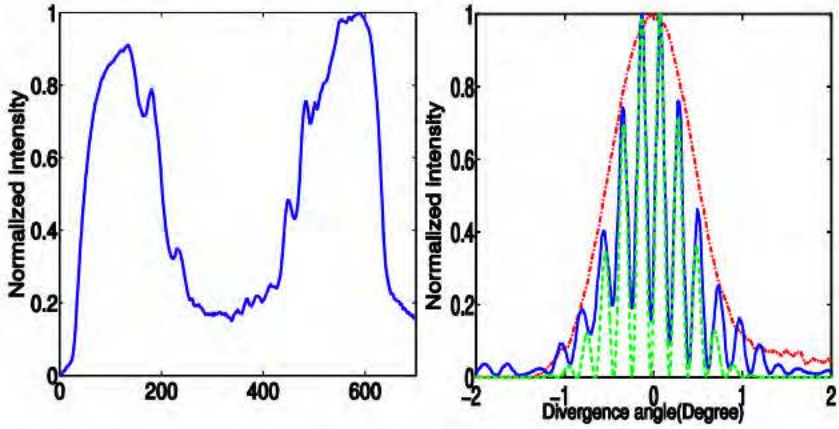

Figure 9 (a) Near field of the coupled laser. (b) Far field profiles: the blue solid line is the measured far field of the coupled laser, the green dashed line is the calculated far field and the red dash-dot line represents the measured far field of a single angled-grating broad-area laser. We obtain a good agreement between the measured and calculated far field.

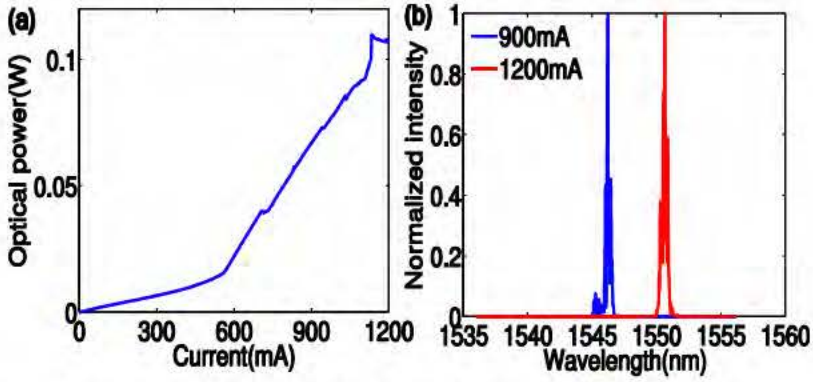

Figure 10 (a) L-I curve. (b) Spectra at two different pump currents.

We also show the comparison between the measured far field (blue solid line) and the calculated result (green dashed line) in Fig. 9(b). The angular distance between fringes in the calculated result is about 0.204^{o}. We obtain a good agreement between the two results. Besides, we also show the measured far field of an ion-implanted single angled-grating broad-area laser. It is presented as the red dash-dot line in Fig. 9(b). In the last section, the divergence angle of the combined laser is slightly larger than that of the single emitter. For our current lasers, however, the envelope of the far field of the combined laser is almost the same as that of the single emitter, which also suggests better coherence. Since there is optical gain in the coupling region, in-phase operation between two emitters should be preferred. However, the two highest peaks with similar intensities in the measured far field seem to indicate out of phase operation. The reason is that due to the misalignment during the die bonding and the positioning errors, the light emitting plane and the far-field measuring plane are not completely parallel and there may be a small angle between these two planes. Since the angular distance between peaks is only about 0.2^{o}, a small angle can affect the measured interference fringes. In the simulation result presented in Fig. 9(b), the two emitters are set to be in phase and we assume the angle between two planes to be ~ 0.1^{o}. The good agreement between the simulation and measurement result indicates that the two emitters are actually in phase.

At last, the measured L-I curve and spectra are shown in Fig. 10. In the L-I curve, the threshold is found to be about 555*mA* and the slope efficiency is about 0.15*W*/*A*. The performance is slightly better than our previous device, benefiting from better current confinement. The kinks in the L-I curve are caused by mode hopping which can be observed in the spectrum measurement shown in Fig. 10(b). When we increase the pump current to about 1200*mA*, the peak wavelength suddenly changes from 1546.2*nm*to 1550.6*nm*.All the near field and far field results were acquired under 1200*mA* pump current condition. When we further increase the pump current, the performance of the laser degrades due to the thermal problem.

In summary, we show the far-field double lobe envelope of our previous lasers is due to the second order Bragg mode. It is excited by the uneven current distribution caused by the lateral current leakage. We use ion implantation to confine the current in the grating area. As a result, better beam quality of the coherently combined angled-grating broad-area lasers is obtained with the near-diffraction-limited, overall single lobe far field. The L-I curve measurement also shows smaller threshold and larger slope efficiency because of better current confinement.

4. Integrated beam combining of laser minibar with six broad area emitters

In the previous two sections, we have demonstrated the monolithic coherent beam combining of two angled-grating broad-area lasers and improved the beam quality of the combined lasers. In this section, we demonstrate integrated coherent beam combining of a laser mini-bar with six angled-grating broad-area lasers based on discrete diffractive coupling. We measure the light-current (L-I) curve, near field, far field and optical spectra of the combined mini laser bar. Near diffraction-limited interference patterns with high contrast ratios are clearly observed in the far field, indicating the excellent spatial coherence among the emitting apertures. The theoretical far field profile is also calculated based on the measured near field profile. The measured far field matches well with the calculated result. The optical spectra of each output aperture exhibit the same lasing wavelengths. These measurement results show that all the six emitters in the mini bar are coherently combined without any external optical components.

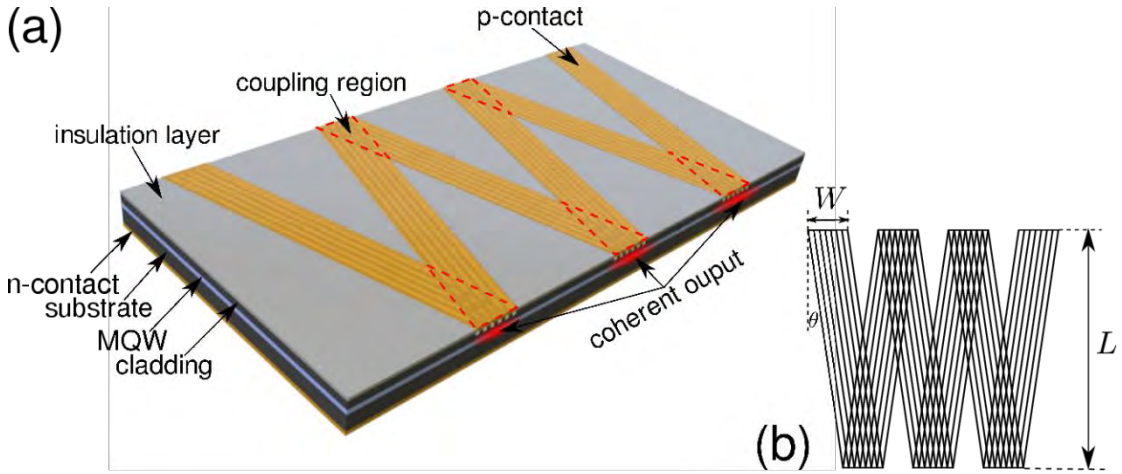

Figure 11 (a) Schematic plot of a mini bar of six coherently combined angled grating broad-area lasers. (b) Diagram of the gratings.

Figure 11 shows the schematic plot of the proposed mini laser bar. We use the angled-grating broad-area laser, which can provide over 1W output power with diffraction-limited beam quality, as the building block. The tilt angle in the design is essential to simultaneously support the snake-like zigzag mode as shown in Fig. 12(a) and eliminate the direct Fabry-Perot(FP) feedback between two end facets. In the proposed array, the neighboring laser diodes tilt to the opposite directions and overlap at one facet. The overlapped areas define several 2D photonic crystal coupling regions. The cavity mode in each individual emitter is the same as that in a single angled-grating broad-area laser. The snake-like zigzag mode as shown in Fig. 12(a) consists of two planewave-like components, denoted by *R*1 and *R*2. The coupling relationship between *R*1/*R*2 and the grating is shown in the inset of Fig. 12. Beam combining of two emitters is obtained through the overlapped coupling region, as shown in Fig. 12(b) for example. The components R_1 and R_1' can be coupled into both R_2 and R_2'through Bragg diffraction. As a result, the energy in one emitter can be coupled into other emitters in the array through the coupling regions.

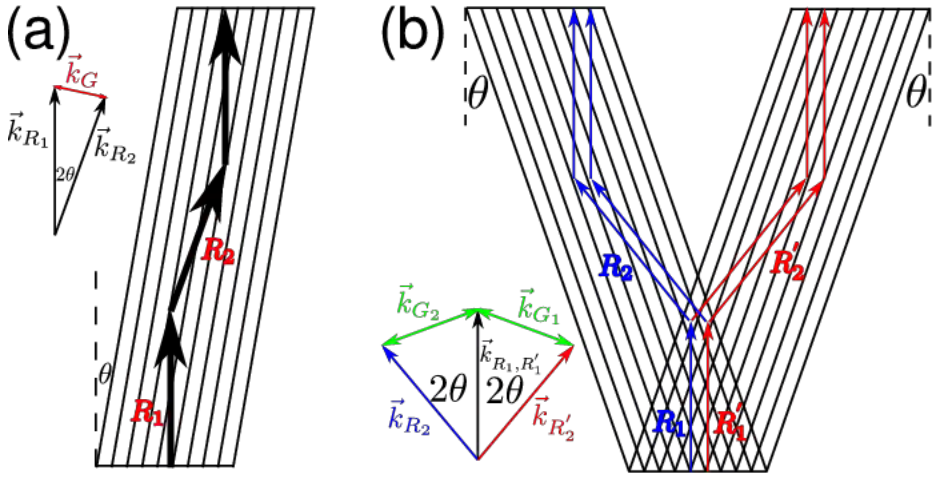

Figure 12 (a) Diagram of the snake-like zigzag mode in an angled-grating broad-area laser. (b) Mode coupling in two combined lasers.

The mini laser bar was fabricated in a InGaAsP multiple quantum well epitaxy wafer. The tilt angle θ is chosen to be $10°$ and the period of gratings is calculated accordingly to be $1.368\mu\mathrm{m}$. The etching depth is

controlled to be around 850*nm* and 100 periods of gratings are etched, resulting in the width (*W*) of about $140\mu m$. The fabrication processes contain several standard steps, including lithography, dry etching, planarization, metallization and ion-implantation. After the chip is lapped to about $100\mu m$ thick, it is cleaved to the length (*L*) of 1.4*mm*. The facets are left uncoated. At last, the laser diodes are die-bonded and wired on a c-mount for measurement. Figure 13 shows scanning electron microscopy (SEM) pictures of the completed device.

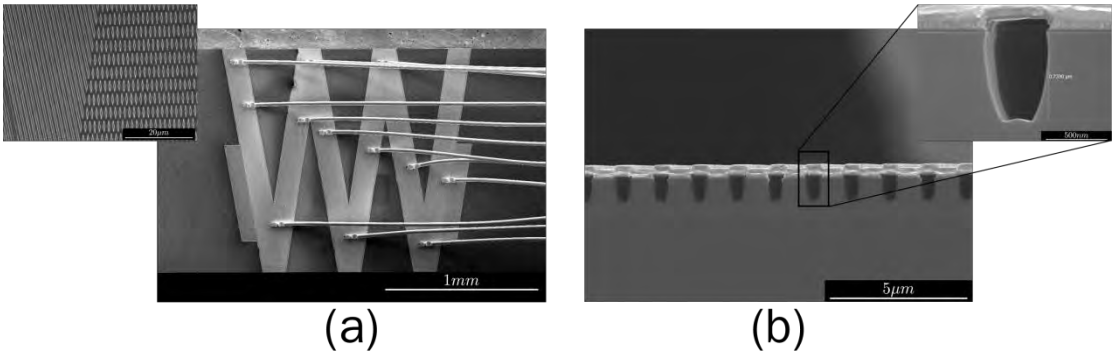

Figure 13 (a) Top view of a completed laser mini bar. The inset is the zoom-in view of the coupling region. (b) Cross-section of the gratings. The inset is the zoom-in view of one tooth of the gratings.

We measured the light-current (L-I) curve, near field, far field and optical spectra of the mini laser bar. All the measurements are carried out with CW current source in a cryostat with the temperature set at 200K to reduce the thermal effect. Figure 14(a) shows the light power vs. current curve of the mini laser bar. The threshold current is about 1213.6*mA*. The slope efficiency is 0.362*W/A* near threshold and changes to 0.247*W/A* at around 2000*mA*. The slope efficiency drop is mainly due to thermal effects since we did not observe the changes in the near field and far field profiles. The maximum power reaches about 650*mW* which is limited by the thermal rollover. In our mini laser bar, the optical spectra of each emitting aperture are measured through the configuration shown in Fig. 15. The laser bar output facet is first imaged through the obj. lenses 1. An iris is placed at the image plane after the obj. lenses 1 as a spatial filter, which lets the light from one aperture pass through and blocks the light from other apertures. This setup ensures that only the light emitting from one aperture can be collimated by the obj. lenses 2 and then collected by the collimator. At last, the collected light is characterized by an optical spectrum analyzer (OSA) through a multi-mode fiber. We first measured the facet with three emitting apertures (see Fig. 11). The optical spectra of the three emitting apertures are shown in Fig. 14 (b). The three apertures have the same lasing wavelengths around 1525.3*nm* with a span of 0.4*nm* as shown in the inset of Fig. 14(b), which indicates good spectral coherence of the mini laser bar.

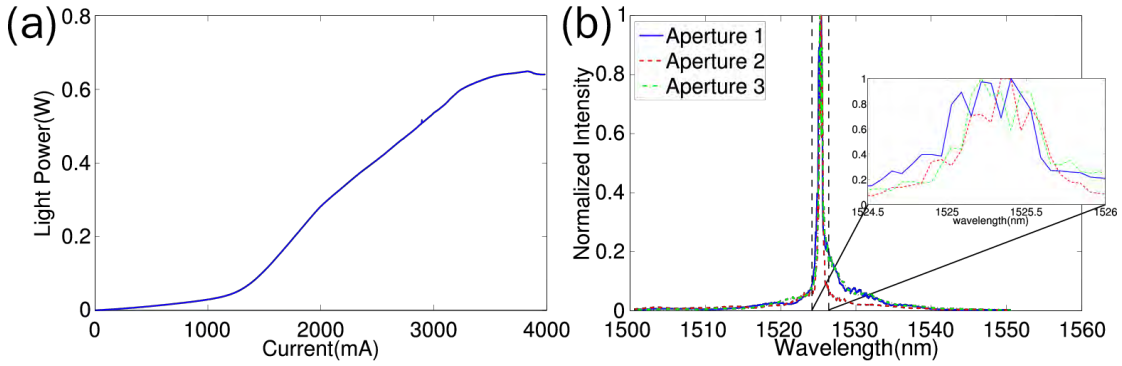

Figure 14 (a) Light power vs. current curve of the mini laser bar. (b) Light spectrum of three apertures at 2000mA; the inset is the zoom-in view between 1524.5nm and 1526nm.

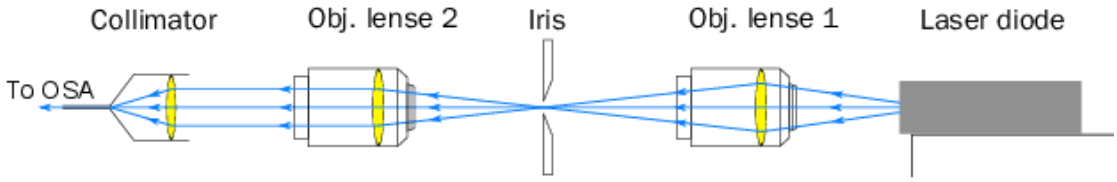

Figure 15 Diagram of the optical setup used to measure the optical spectrum of each aperture.

The fabricated mini laser bar has two output facets. One contains three apertures and each of them consists of the combination of two emitters. At the other side, the two middle apertures consist of the combined outputs and the other two aside only consist of the output of one laser diode. Figure 16(a) shows the near field profile measured at the three-aperture facet. In this figure, the distances between the neighboring apertures are very close to each other and match well with the design parameters. The similar intensities and widths of the three apertures indicate an uniform distribution of injected current. These values are denoted in this figure and used to calculate the theoretical far field profiles. In Fig. 16(b), we show the measured and calculated far field profiles, along with the far field profile of a single angled-grating broad-area laser. High contrast ratio interference fringes are clearly observed in this figure. The measured average angular distance between fringes is about 0.2093° which is very close to the theoretical result of 0.2077°. The measured FWHM of the far field is about 1.5° which is slightly larger than the calculated result of 1.1°. All the results above demonstrate that the mini laser bar is coherently combined with near diffraction-limited beam quality. Figure 17 shows the near field and far field measurement results of the four-aperture side, respectively. In the near field profile, the two side apertures have slightly smaller intensities than the two middle apertures. Interference fringes are clearly observed in the far field profile as well, indicating good spatial coherence of this emitting facet. We also observe some non-uniform spikes in the near field profile of two side apertures. We consider the reason as follows. When cleaved, the polymer used for planarizing the gratings may not break uniformly along the cleavage plane of the substrate and some of them stretch out in front of the laser facet. These polymer causes scattering of the output light resulting in the spikes in the near field.

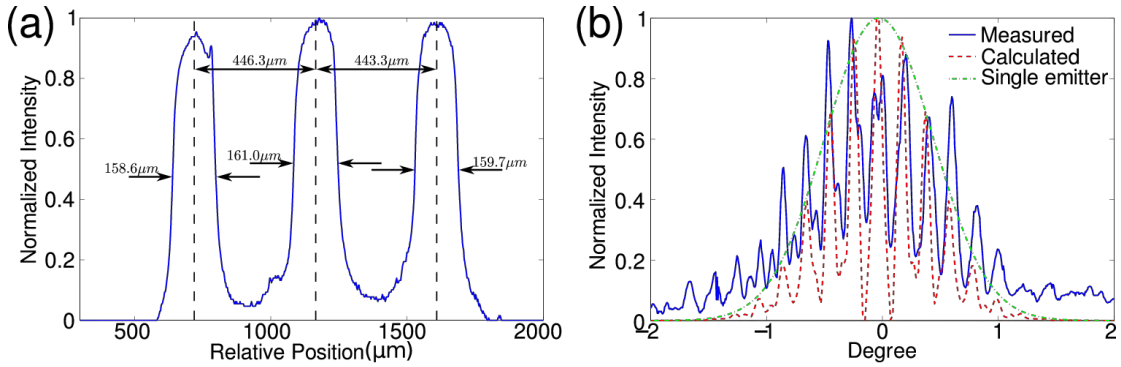

Figure 16 Near field and far field profiles of the three coherent output apertures of a mini-bar at 2000mA. (a) Near field profile. (b) Measured far field profile (blue solid line); calculated far field profile (red dashed line); far field profile of a single angled-grating broad-area laser (green dash-dotted line).

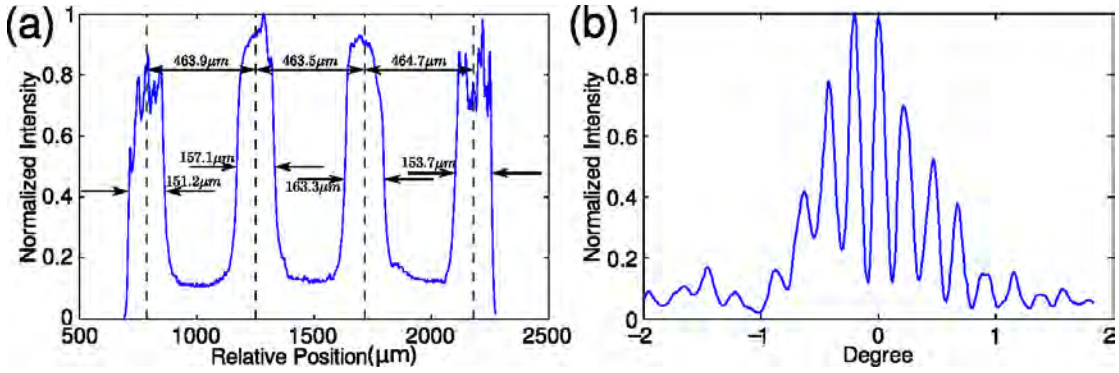

Figure 17 Near field and far field profiles of the four coherent output apertures of a mini-bar at 2000mA. (a) Near field profile. (b) Measured far field profile

In summary, we demonstrate the coherent beam combining of a mini laser bar of six angled-grating broad-area lasers with near diffraction-limited beam quality. The fabricated laser bar exhibits high contrast ratio interference fringes in far field, indicating excellent spatial coherence. The measured optical spectra of each individual output aperture show the same lasing wavelengths. The L-I curve shows that the maximum power is limited by the thermal effect. All the experimental results prove that the proposed mini laser bar is coherently combined with near diffraction-limited beam quality without any external components or feedback.

5. Conclusions

This YIP project has successfully demonstrated integrated mode control and coherent beam combining of high power, broad area lasers through transverse Bragg diffractions. The proposed concept has many advantages over traditional beam combining methods based on discrete and bulky optical components. It is clear that the proposed approach can effectively realize the single mode operation of broad-area diode lasers and coherently combine these angled-grating lasers with high efficiency. The current challenge is that the devices are operating at relatively low temperatures and the total output power is less than a couple watts. We believe that this problem is mainly due to the scattering and non-radiative losses induced by the deeply etched gratings. We are currently working on greatly improve the device performance through the grating regrowth and 2D grating designs.

Reference:

[1] R. Poprawe, P. Loosen, and F. Bachmann, High Power Diode Lasers, Springer, 2007
[2] R. Diehl, High-Power Diode Lasers: Fundamentals, Technology, Applications, Springer, 2010
[3] H. Li et al., "Near 1 kW of continuous-wave power from a single high-efficiency diode-laser bar", IEEE Photon. Technol. Lett. 19, 960-962, 2007
[4] D. F. Welch, "A brief history of high power semiconductor lasers," IEEE J. Select. Topics Quantum Electron. , 6, 1470-1477, 2000
[5] J. Lim, et al., "Design and simulation of next-generation high-power, high-brightness laser diodes," IEEE J. Select. Topics Quantum Electron. , 15, 993-1008, 2009
[6] C. M. Stickley, M. E. Filipkowski, E. Parra, and M. Sandrock, "High power laser diodes and applications to direct diode HELs" LEOS Annual Meeting, 468-469, 2006
[7] L. A. Coldren and S. W. Corzine, Diode Lasers and Photonic Integrated Circuits, Wiley Interscience, 1995
[8] G. P. Agrawal and N. K. Dutta, Long-wavelength Semiconductor Lasers, Van Nostrand Reinhold, 1986
[9] D. Botez and D. R. Scifres, Diode laser arrays, Cambridge University Press, 1986
[10] A. H. Paxton and G. C. Dente, "Filament formation in semiconductor-laser gain regions," J. Appl. Phys., 70, 2921-2925, 1991
[11] D. F. Welch, D. R. Scifres, P. S. Cross, H. Kung, W. Streifer, R. D. Burnham, and J. Yaeli, "High power (575 mW) single-lobed emission from a phased-array laser," Electron. Lett., 21, 603-604, 1985
[12] D. R. Scifres, R. D. Burnham, and W. Streifer, "Phase-locked semiconductor laser array," Appl. Phys. Lett., 33, 1015-1017, 1978
[13] D. E. Ackley, "Single longitudinal mode operation of high power multiple-stripe injection laser," Appl. Phys. Lett., 42, 152-154, 1983
[14] E. Kapon, J. Katz, and A. Yariv, "Supermode analysis of phase locked arrays of semiconductor lasers," Opt. Lett., 10, pp. 125-127, 1984
[15] J. K. Butler, D. E. Ackley, and M. Ettenberg, "Coupled-mode analysis of gain and wavelength oscillation characteristics of diode laser phased arrays," IEEE J. Quantum Electron., 21, pp. 458-463, 1985
[16] D. F. Welch, P. S. Cross, D. R. Scifres, W. Streifer, and R. D. Burnham, "High power (cw) in-phase locked 'Y' coupled laser arrays," Appl Phys. Lett., 49, 1632-1634, 1986
[17] D. Botez P. Hayashida, L. J. Mawst, and T. J. Roth, "Diffraction-limited-beam, high-power operation from X-junction coupled phase-locked arrays of AlGaAs/GaAs diode lasers," Appl. Phys. Lett. 53, 1366-1368,1988
[18] B. Hermansson and David Yevick, "Analysis of Y-junction and coupled laser arrays," Applied Optics, 28, 66-73, 1989
[19] D. Botez, L. J. Mawst, G. Peterson, and T. J. Roth, "Resonant optical transmission and coupling in phase-locked diode laser arrays of antiguides: The resonant optical waveguide array," Appl. Phys. Lett., 54, 2183-2185, 1989
[20] C. Zmudzinski, D. Botez, and L. J. Mawst, "Coherent, one watt operation of large-aperture resonant arrays of antiguided diode lasers," Appl. Phys. Lett., 62, 2914-2916, 1993
[21] H. Yang, L. J. Mawst, M. Nesnidal, J. Lopez, A. Bhattacharaya, and D. Botez, "Ten watt, near-diffraction-limited peak pulse power from Al free, 0.98 micron emitting, phase-locked, antiguided arrays," Electron. Lett., 33,136-137, 1997
[22] J. Salzman, T. Venkatesan, S. Margalit, and A. Yariv, "An unstable resonator semiconductor laser," Optical Societyof America Meeting, San Diego, CA, paper ThV3, 1984
[23] M. L. Tilton, G. C. Dente, A. H. Paxton, J. Cser, R. K. DeFreez, C. E. Moeller, and D. Depatie, "High power, nearly diffraction-limited output from a semiconductor laser with an unstable resonator," IEEE J. Quantum Electron., 27, 2098-2108, 1991

[24] E. S. Kintzer, J. N. Walpole, S. R. Chinn, C. A. Wang, and L. J. Missaggia, “High power strained layer amplifiers and lasers with tapered gain regions,” IEEE Photon. Technol. Lett., vol. 5, pp. 605–608, 1993.
[25] Z. Bao, R. K. DeFreez, P. D. Carleson, C. Largent, C. Moeller, and G. C. Dente, “Spatio-spectral characteristics of a high power, high brightness CW InGaAs/AlGaAs unstable resonator semiconductor laser,” Electron.Lett., vol. 29, no. 18, pp. 1597–1599, 1993.
[26] D. Masanotti and F. Causa, “Optical guiding properties of high-brightness parabolic bow-tie laser arrays,” IEEE J. Quantum Electron., 41, 909-916, 2005
[27] D. Mehuys, D. F. Welch, R. Parke, R. G. Waarts, A. Hardy, and D. R. Scifres, “High power diffraction-limited emission from monolithically integrated active grating master oscillator power amplifier,” Electron. Lett., 27, 492-494, 1991
[28] N. W. Carlson, J. H. Abeles, D. P. Bour, S. K. Liew, W. F. Reichert, P. S. D. Lin, and A. S. Gozdz, “Demonstration of a monolithic grating surface-emitting laser master oscillator cascaded power amplifier array,” IEEE Photon. Technol. Lett., 2, 708-710, 1990
[29] R. Parke, D. F. Welch, A. Hardy, R. Lang, D. Mehuys, S. Obrien, K. Dzurko, and D. Scifres, “2.0 W CW, diffraction-limited operation of a monolithically integrated master oscillator power-amplifier,” IEEE Photon. Technol. Lett., 5, pp. 297-300, 1993
[30] S. Wang and S. Sheem, “Two-dimensional distributed-feedback lasers and their applications,” Appl. Phys. Lett. , 22, 460-462, 1973
[31] R. J. Lang, K. D. Zurko, A. Hardy, S. Demars, A. Schoenfelder, and D. Welch. “Theory of grating-confined broad-area lasers,” IEEE J. Quantum Electron., 34 2196-2210, 1998
[32] A. M. Sarangan, M. W. Wright, J. Marciante, and D. J. Bossert, “Spectral properties of angles-grating high-power semiconductor lasers,” IEEE J. Quantum Electron., 35, 1220-1230, 1999.
[33] W. W. Bewley, I. Vurgaftman, R. E. Bartolo, M. J. Jurkovic, C. L. Felix, J. R. Meyer, H. Lee, R. U. Martinelli, G. W. Tuner, and M. Manfra, “Limitations to beam quality of mid-IR angled-grating distributed feedback lasers,” IEEE J. Select. Topics Quantum Electron., 7, 96-101, 2001.
[34] I. Vurgaftman and J. R. Meyer, “Photonic-crystal distributed-feedback quantum cascade lasers,” IEEE J. Quantum Electron. , 38, 592-602, 2002
[35] K. Paschke, A. Bogatov, F. Bugge, A. E. Drakin, J. Fricke, R. Guther, A. A. Stratonnikov, H. Wenzel, and G. Erbert, “Properties of ion-implanted high-power anged-grating distributed-feedback lasers,” IEEE J. Select. Topics Quantum Electron., 9, 1172-1178, 2003
[36] A. Yariv, Y. Xu, and S. Mookherjea, “Transverse Bragg resonance (TBR) laser amplifier,” Opt. Lett. , 28, 176-178, 2003
[37] C. S. Kim, W. W. Bewley, C. L. Canedy, I. Vurgaftman, M. Kim, and J. R. Meyer, “Broad-stripe near-diffraction-limited mid-infrared laser with a second-order photonic-crystal distributed feedback grating,” IEEE Photon. Tech. Lett. , 16, 1250-1252, 2004
[38] L. Zhu, G. A. DeRose, A. Scherer, and A. Yariv, “Electrically-pumped, edge-emitting photonic crystal lasers with angled facets,” Opt. Lett., 32, 1256-1258, 2007
[39] L. Zhu, A. Scherer, and A. Yariv, “Modal gain analysis of transverse Bragg resonance waveguide lasers with and without transverse defects,” IEEE J. Quantum Electron., 43, 934-940, 2007
[40] L. Zhu, X. K. Sun, G. A. DeRose, A. Scherer, and A. Yariv, “Room temperature continuous wave operation of single-mode, edge-emitting photonic crystal Bragg lasers,” Optics Express, 16, 502-506, 2008
[41] C. Hasnain, D. F. Welch, D. R. Scifres, J. R. Whinnery, A. Dienes, and R. D. Burnham, “Diffraction-limited emission from a diode laser array in an apertured graded-index lens external
cavity,” Appl. Phys. Lett. 49, 614-616, 1986
[42] G. A. Henderson and D. L. Begley, “Injection-locked semiconductor laser array using a graded-index rod: a computational model,” Applied Optics, 28, 4548-4551, 1989

[43] J. R. Leger, “Lateral mode control of an AlGaAs laser array in a Talbot cavity,” Appl. Phys. Lett., 55, 334-336, 1989
[44] R. Waarts, D. Mehuys, D. Nam, D. Welch, W. Streifer, and D. Scifres, “High-power, cw, diffraction-limited, GaAlAs laser diode array in an external Talbot cavity,” Appl. Phys. Lett. 58, 2586-2588, 1991
[45] J. R. Leger and G. Mowry, “External diode-laser-array cavity with mode-selecting mirror,” Appl. Phys. Lett. 63, 2884-2886, 1993
[46] L. Goldberg, J. F.Weller, D. Mehuys, D. F.Welch, and D. R. Scifres, “12W broad area semiconductor amplifier with diffraction-limited optical output,” Electron. Lett., 27, 927-929, 1991
[47] J. N. Walpole, E. S. Kintzer, S. R. Chinn, C. A. Wang, and L. J. Missaggia,“High-power strained-layer InGaAs/AlGaAs tapered traveling wave amplifier,” Appl. Phys. Lett., 61, 740-742, 1992
[48] D. Mehuys, D. Welch, and D. Scifres, “1 W diffraction-limited tunable external cavity semiconductor laser,” Electron. Lett., 29, 1254-1255, 1993
[49] T. Y. Fan, “Laser beam combining for high-power, high-radiance sources,” IEEE J. Select. Topics Quantum Electron., 11, 567-577, 2005
[50] J. R. Leger, M. Holz, G. J. Swanson, and W. Veldkamp, “Coherent beam addition: An application of binary optics,” Lincoln Lab. J., 1, 225-245, 1988
[51] A. F. Glova, “Phase locking of optically coupled lasers,” Quantum Electron., 33, pp. 283–306, 2003
[52] V. Daneu, A. Sanchez, T. Y. Fan, H. K. Choi, G. W. Turner, and C. C. Cook, “Spectral beam combining of a broad-strip diode laser array in an external cavity,” Opt. Lett. 25, 405-407, 2000
[53] B. Chann, R. K. Huang, L. J. Missaggia, C. T. Harris, Z. L. Liau, A. K. Goyal, J. P. Donnelly, T. Y. Fan, A. Sanchez-Rubio, and G. W. Turner, “Near-diffraction-limited diode laser arrays by wavelength beam combining,” Opt. Lett. 30, 2104-2106, 2005
[54] O. Andrusyaka, V. Smirnovb, G. Venusa and L. Glebov, “Beam combining of lasers with high spectral density using volume Bragg gratings,” Optics Communications 282, 2560-2563, 2009
[55] S. J. Augst, T. Y. Fan, and A. Sanchez, “Coherent beam combining and phase noise measurements of ytterbium fiber amplifiers,” Opt. Lett., 29, 474-476, 2004
[56] W. Liang, N. Satyan, F.Aflatouni, A.Yariv, A. Kewitsch, G. Rakuljic, and H. Hashemi, “Coherent beam combining with multilevel optical phase-locked loops,” J. Opt. Soc. Am. B 24, 2930-2939, 2007
[57] A. A. Ishaaya, N. Davidson, and A. A. Friesem, “Passive laser beam combining with intracavity interferometric combiners,” IEEE J. Select. Topics Quantum Electron., 15, 301-311, 2005